Indian Journal of Chemical Technology
Vol. 33, May 2026, pp. 444-455
DOI: 10.56042/ijct.v33i3.21958

Influence of EMHD flow of a non-Newtonian ternary hybrid nanofluid over a variable thickness surface with thermal effects and Cattaneo-Christov heat flux: Applications in biomedical engineering

Kaleeswari M[1], Kotte Amaranadha Reddy[1*], Maduru Lakshmi Rupa[2], Seethi Reddy Reddisekhar Reddy[3] & Shaik Jakeer[4]

[1]Department of Mathematics, School of Advanced Science, Kalasalingam Academy of Research and Education, Virudhunagar - 626126, Tamil Nadu, India

[2]Department of Mathematics, CMR Institute of Technology, Hyderabad 501401, Telangana, India

[3]Department of Mathematics, Koneru Lakshmaiah Education Foundation, Bowrampet, Hyderabad, 500043, Telangana, India

[4]School of Technology, The Apollo University, Chittoor – 517127, Andhra Pradesh, India

*E-mail: amar.anil159@gmail.com

Received 24 July 2025; accepted 2 March 2026

This article investigates a Darcy-Forchheimer flow nonlinear analysis in an electro-magnetohydrodynamic regime for a non-Newtonian ternary hybrid nanofluid (Cu–Fe_3O_4–Ti/blood) over a slanting extending plate incorporated in a porous medium, considering consistent heat source and sink effects and linear TR. By substituting the Cattaneo–Christov (CC) heat flow model for the traditional Fourier law, a thermal relaxation time permits limited-speed thermal signal transmission, thereby incorporating a more physically realistic heat conduction process. The boundary layer governing equations are transformed into a collection of nonlinear ordinary differential equations (ODEs) with the help of transformations of similarity, and these are then numerically resolved using MATLAB's bvp4c solver. The impact of inclination angle, electromagnetic parameters, volume fractions of nanoparticles, and thermal relaxation time on flow and heat transmission characteristics is demonstrated using parametric testing. The findings recommend prospective uses in targeted medication administration, thermal therapy, and bio-microfluidic devices in biomedical engineering by exhibiting improved thermal conductivity and controlled heat propagation.

Keywords: Cattaneo-Christov heat flux, Convective boundary condition, Darcy-Forchheimer, EMHD, Variable thickness surface, Porous medium

Introduction

In contrast to classical Fourier's law, the CC model of heat flux is a non-Fourier heat conduction model that considers the thermal relaxation time of the medium and ensures finite-speed propagation of heat. It is especially helpful in fast, small-scale, or complex systems like nanofluids, high-speed flows, biological tissues, and MHD applications. Incorporating time delay (Cattaneo) and frame invariance (Christov) into the model improves its accuracy, making it essential for accurate transient heat transfer analysis in sophisticated thermal systems[1-10]. Li *et al.*[1] analyzed thermal transmission in a THNF (AlO_3–Ag–CuO/water) across an extending sheet using the CC heat flux model. Significant effects are examined, such as magnetic fields, heat radiation, and nanoparticle shapes. Reddy and Bala[2] investigated how radiation affects the unstable MHD micropolar flow across a thinned plate. To describe the obtained mathematical model, the homotopy perturbation method and the numerical method were proposed. Sharjeel and Sagheer[3] demonstrated how magnetic fields and concentrations of silver nanoparticles raise temperature while reducing flow velocity and heat transfer in their study of MHD flow of a THNF over an extended sheet with slip and non-Fourier heat flux. Sandhya Rani *et al.*[4] investigated the movement of chemically reactive nanofluids over a stretched plate using Joule heating and CC heat flux. The thickness of the boundary layer was found to be increased by the significant influence of magnetic fields, permeability, and thermal factors on temperature and velocity profiles. Reddy *et al.*[5] used the CC heat flux model to examine how the energy of activation affects the chemical reaction of Eyring-Powell nanofluid past an angled radiative cylinder. Abdal *et al.*[6] suggested that fluid properties and magnetic fields have a major impact on flow and temperature behaviour. They

looked into how heat transmission over an extended sheet can be enhanced by nanofluids with Maxwell and bioconvection and CC heat flux. Iqbal *et al.*[7] observed that buoyancy and mixed convection increased velocity while magnetic fields decreased it in their investigation of Maxwell flow of fluid over an extending plate with CC heat flux. Shankaralingappa *et al.*[8] addressed relaxation chemical processes, thermophoretic particle deposition, and CC dual diffusion in their study of Oldroyd-B flow of fluid across an extending plate. It used numerical approaches to show how diverse variables affected the concentration, velocity, and temperature profiles. Using the Cattaneo–Christov model, Abbas *et al.*[9] evaluated the movement and transfer of heat of a Williamson fluid over an extending plate in a porous media. The results, which were accomplished using a numerical shooting approach, suggested that the concentration, velocity, and temperature profiles were considerably impacted by slip velocity, viscosity, and chemical reactions. Khalil *et al.*[10] examined how various properties affected the fluid and the dual diffusive CC model on the heat transmission and flow of a Powell–Eyring fluid over an extending sheet using numerical techniques, which showed the effect of thermal conductivity, viscosity, and chemical reactions.

Non-Newtonian nanofluids are being extensively investigated for implementation in industrial processes, electronics cooling, and biological systems due to their changeable viscosity and enhanced thermal properties. Nanoparticles like TiO_2, Cu, or Al_2O_3 are added to non-Newtonian-based fluids to improve their stability and heat conductivity. They are used in a wide range of sectors, and even Newtonian base fluids can exhibit non-Newtonian behaviour when nanoparticles are added. Abbas *et al.*[11] used numerical analysis to study the heat propagation and flow of a second-grade NF over an exponentially permeable extending curved Riga sheet, demonstrating the effects of chemical reactions, porosity, and magnetic fields on temperature, velocity, and concentration profiles. Elgazery and Asmaa[12] had evaluated the flow of a Casson non-Newtonian NF over an extending sheet with nonlinear TR. Only the first solution was found to be stable, illustrating how factors like thermophoresis and resistance to porous media affected the concentration, velocity, and temperature of nanoparticles. Reddy and Bala[13] numerically investigated the unstable micropolar 3D MHD flow over a thin stretching plate. In their exploration of 3D MHD flow of a non-Newtonian NF over a porous, extending plate with nonlinear TR and heat absorption, Tarakaramu *et al.*[14] explored that heat transfer, velocity, and concentration profiles were significantly impacted by magnetic fields, porosity, and thermophysical parameters. Tuesday *et al.*[15] discovered the unsteady hydromagnetic movement of a non-Newtonian NF via a porous extending sheet and showed that magnetic fields, chemical reactions, and various flow parameters significantly affected the fluid's concentration, velocity, and temperature profiles. The impact of chemically reacting hydromagnetic flow across an incline with exponential stretching was examined by Reddy and Bala[16], utilising unequal gain or loss. Maxwell NF flowed over an extending rough plate via porous media, and it was viewed that viscous dissipation, slip velocity, and thermophysical variables significantly affected the concentration, velocity and temperature profiles analyzed by Amer *et al.*[17]. Xin *et al.*[18] observed that heat transmission, fluid velocity, and pollutant concentration were significantly influenced by nanoparticles, thermal radiation, and fluid properties in their study of the release of pollutants through a porous Riga sheet in non-Newtonian NF flow. Ramesh *et al.*[19] analyzed the EMHD flow of an iron oxide, titanium oxide, and extending surface with an HNF of ethylene glycol and observed that radiation increased temperature, magnetic fields reduced velocity, and hybrid nanofluids enhanced heat transfer performance. Abbas *et al.*[20] proved that thermal slip, suction, and micropolar effects all significantly influenced the temperature, velocity, and concentration profiles in their investigation of micropolar NF flow over an incredibly extended sheet. A substance's porosity, or the amount of empty space inside it, determines how efficiently it holds or transports fluids. By being essential to fluid flow, heat transmission, and mechanical strength, porosity influences fields such as geology, civil engineering, thermal systems, and biomedical applications. In porous media, increased porosity enhances fluid penetration and heat exchange while influencing permeability, strength, and thermal behaviour.

Yousef *et al.*[21] observed the influence of chemical processes, fields of magnet, and slip velocity on the HMT of a Casson-Williamson NF through an extending plate in a porous medium. They discovered

that magnetic and porous effects slowed the flow and reduced heat transfer, whereas chemical interactions enhanced mass transfer. Mondal *et al*.[22] found how magnetic fields, thermophoresis, Soret-Dufour effects, and chemical reactions significantly altered flow, temperature, and concentration behaviours when they explored their effects on HMT across an inclined plate. Amer *et al*.[23] delved into tangent hyperbolic NF flow along an extending plate within a porous medium with slip and magnetic effects. They determined that raising the magnetic field, slip, and porosity raises their temperature and concentration while decreasing velocity. This has important applications in heat exchangers and material processing. Raza *et al*.[24] explored the MHD movement of a Williamson NF over an elongated sheet with variable thickness and noticed that temperature, velocity, and concentration of nanoparticles were significantly influenced by TC, Brownian motion, magnetic fields, slip influence, and thermophoresis. These factors, in turn, influenced the rates of HMT. CF flow with magnetic field effects, CR, and suction over an elongated sheet in a porous medium, exhibiting that key parameters influence velocity and concentration profiles, was discussed by Ekang *et al*.[25]. Kayalvizhi and Vijaya Kumar[26] concluded that magnetic fields reduced velocity, while electric fields and radiation enhanced temperature and entropy generation in their study of EMHD HNF flow along a porous elongated sheet. Qamar *et al*.[27] explored EMHD bio-NF flow across an extending sheet through the Galerkin FEM and revealed that magnetic, electric, and thermal phenomena significantly impacted fluid behaviour and HMT. Faisal *et al*.[28] evaluated MHD Hiemenz flow across a nonlinear stretched sheet and showed that magnetic fields and chemical reactions reduced flow and concentration while radiation and thermophoresis increased temperature. A Cu-CNT-Ti/water THNF heat transfer under thermal and electromagnetic effects was evaluated by Shaik Jakeer *et al*.[29], which indicated better thermal performance than conventional nanofluids. Because of its unique rheological properties, the Casson fluid is a remarkable representation of non-Newtonian NF that finds application in the fields of engineering and biology. This model is very significant in cases involving fluid dynamics in magnetic fields, heat transfer, and drug delivery. The CF model, which Casson introduced in 1959, describes the flow behaviour of viscoplastic fluids, which can be both solid and liquid depending on the stress applied. Because it accurately depicts the flow characteristics of blood, chocolate, and even printing ink, this model has found usage in various fields, such as polymer production, culinary science, and biomedical engineering.

A prior study based on the literature found that there had been no attempt to illustrate the non-linear Darcy-Forchheimer flow in EMHD of aTHNF while incorporating non-Fourier heat conduction. HT characteristics of copper, Iron oxide, and titanium with blood over an elongated sheet with linear TR, a porous medium, a homogenous heat source/sink, and a CC heat flow model are the main applications of this model. Compared to the traditional Fourier law, this enhanced heat conduction model improves the accuracy of thermal forecasts by considering thermal relaxation time, which permits finite-speed propagation of thermal disturbances. The current model may be used in the key technologies for sustainable energy and environmental systems, such as hydrogen generation, wastewater treatment, drug delivery, and biodiesel synthesis. MATLAB's bvp4c solver technique is utilised to solve the system of ODEs that result from similarity variables of the governing fluid transport equations. This process incorporates the influence of non-Newtonian NF behaviour and non-Fourier heat flow. A detailed discussion and graphic illustrations of the results are provided. Future research might concentrate on expanding this framework to include more generalisations to time-dependent or three-dimensional geometries.

Mathematical Modelling

The Cattaneo–Christov heat flux model is employed to analyse the 2D nonlinear electro magnetohydrodynamic flow of an incompressible, laminar ternary hybrid Casson nanofluid (Cu–Fe_3O_4–Ti/blood) over a variable thickness surface, as illustrated in Fig. 1. The surface is non-flat and is described by the profile $y = \left(\sqrt{x+c}\right)^{1-n} J,$. The surface exhibits an outer concave shape when $n < 1$ and an inner convex shape when $n > 1$. Furthermore, a uniform magnetic and electric field is applied vertically to the inclined surface. We also analysed the implications of viscous dissipation and Joule heating under convective boundary conditions. The

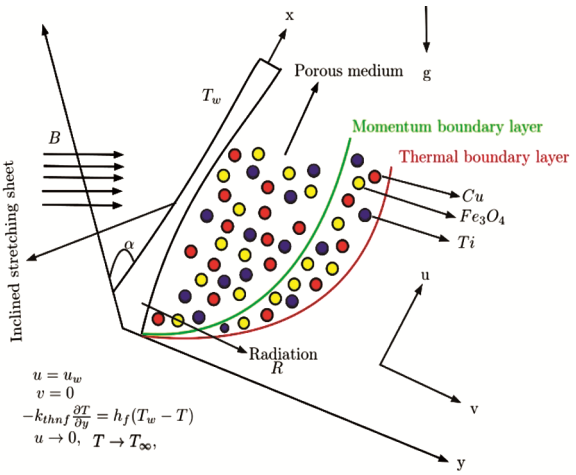

Fig. 1 — Schematic illustration of the required problem

mathematical representation for the sheet surface's variable thickness velocity is $u_w = U_0(c+x)^n$. The boundary layer flow equations for the THNF are given as follows[1,12,16,29].

$$\frac{\partial u}{\partial x}+\frac{\partial v}{\partial y}=0, \qquad \ldots (1)$$

$$\left.\begin{aligned} u\frac{\partial u}{\partial x}+v\frac{\partial u}{\partial y}=\upsilon_{thnf}\left(1+\frac{1}{\beta}\right)\frac{\partial^2 u}{\partial y^2}+(T-T_\infty)g\cos(\alpha)(\beta_T)_{thnf} \\ -\frac{\sigma_{thnf}B}{\rho_{thnf}}(Bu-E_0)-\frac{\upsilon_{thnf}}{k'}\left(1+\frac{1}{\beta}\right)(u)-\frac{F^*}{k'}(u^2), \end{aligned}\right\} \qquad \ldots (2)$$

$$\begin{aligned} u\frac{\partial T}{\partial x}+v\frac{\partial T}{\partial y}+\varepsilon_t\left[\begin{aligned} &u^2\frac{\partial^2 T}{\partial x^2}+2uv\frac{\partial^2 T}{\partial x\partial y}+v^2\frac{\partial^2 T}{\partial y^2}+u\frac{\partial u}{\partial x}\frac{\partial T}{\partial x}+ \\ &v\frac{\partial u}{\partial y}\frac{\partial T}{\partial x}+u\frac{\partial v}{\partial x}\frac{\partial T}{\partial y}+v\frac{\partial v}{\partial y}\frac{\partial T}{\partial y} \end{aligned}\right] \\ =\alpha_{thnf}\frac{\partial^2 T}{\partial y^2}+\frac{16\sigma^* T_\infty^3}{(\rho C_p)_{thnf}3k_1^*}\frac{\partial^2 T}{\partial y^2}+\frac{\mu_{thnf}}{(\rho C_p)_{thnf}}\left(1+\frac{1}{\beta}\right)\left(\frac{\partial u}{\partial y}\right)^2 \\ +\frac{\sigma_{thnf}}{(\rho C_p)_{thnf}}(Bu-E_0)^2+\frac{Q^*}{(\rho C_p)_{thnf}}(T-T_\infty) \end{aligned} \qquad \ldots (3)$$

The essential boundary conditions[1,29] are as follows:

$$u = u_w, v = 0, -k_{thnf}\frac{\partial T}{\partial y} = h_f(T_w - T),$$

$$\text{at } y = \left(\sqrt{x+c}\right)^{1-n} J, \qquad \ldots (4)$$

$$u \to 0, T \to T_\infty, \text{ as } y \to \infty,$$

Where

$$B = B_0\left\{(c+x)^{\frac{1}{2}}\right\}^{(n-1)}, k' = k_0'(c+x)^{-(n-1)}, \qquad \ldots (5)$$

$$Q^* = Q_0(c+x)^{(n-1)}, T_W = T_\infty + T_0(c+x)^{(1-n)0.5}.$$

The THNF has the following thermophysical characteristics[29]:

Density

$$\frac{\rho_{\text{thnf}}}{\rho_{\text{bf}}} = (1-\phi_3)\left((1-\phi_2)\left(1-\phi_1+\phi_1\frac{\rho_{np1}}{\rho_{bf}}\right)+\phi_2\frac{\rho_{np2}}{\rho_{bf}}\right)+\phi_3\frac{\rho_{np3}}{\rho_{bf}}$$

Thermal volumetric expansion

$$\frac{(\rho\beta_T)_{\text{thnf}}}{(\rho\beta_T)_{bf}} = (1-\phi_3)\left(\begin{aligned}&(1-\phi_2)\left(1-\phi_1+\phi_1\frac{(\rho\beta_T)_{np1}}{(\rho\beta_T)_{bf}}\right)\\&+\phi_2\frac{(\rho\beta_T)_{np2}}{(\rho\beta_T)_{bf}}\end{aligned}\right)+\phi_3\frac{(\rho\beta_T)_{np3}}{(\rho\beta_T)_{bf}}$$

Heat capacitance

$$\frac{(\rho c_p)_{\text{thnf}}}{(\rho c_p)_{bf}} = (1-\phi_3)\left((1-\phi_2)\left(1-\phi_1+\phi_1\frac{(\rho c_p)_{np1}}{(\rho c_p)_{bf}}\right)+\phi_2\frac{(\rho c_p)_{np2}}{(\rho c_p)_{bf}}\right)+\phi_3\frac{(\rho c_p)_{np3}}{(\rho c_p)_{bf}}$$

Thermal conductivity

$$k_{\text{nf}} = \frac{\left(k_{np1}+2k_{bf}-2\phi_1\left(k_{bf}-k_{np1}\right)\right)k_{bf}}{k_{np1}+2k_{bf}+\phi_1\left(k_{bf}-k_{np1}\right)},$$

$$k_{\text{hnf}} = \frac{\left(k_{np2}+2k_{nf}-2\phi_2\left(k_{nf}-k_{np2}\right)\right)k_{nf}}{k_{np2}+2k_{nf}+\phi_2\left(k_{nf}-k_{np2}\right)},$$

$$k_{\text{thnf}} = \frac{\left(k_{np3}+2k_{hnf}-2\phi_3\left(k_{hnf}-k_{np3}\right)\right)k_{hnf}}{k_{np3}+2k_{hnf}+\phi_3\left(k_{hnf}-k_{np3}\right)}.$$

Electrical conductivity

$$\sigma_{\text{nf}} = \frac{\left(\sigma_{np1}+2\sigma_{bf}-2\phi_1\left(\sigma_{bf}-\sigma_{np1}\right)\right)\sigma_{bf}}{\sigma_{np1}+2\sigma_{bf}+\phi_1\left(\sigma_{bf}-\sigma_{np1}\right)},$$

$$\sigma_{\text{hnf}} = \frac{\left(\sigma_{np2}+2\sigma_{nf}-2\phi_2\left(\sigma_{nf}-\sigma_{np2}\right)\right)\sigma_{nf}}{\sigma_{np2}+2\sigma_{nf}+\phi_2\left(\sigma_{nf}-\sigma_{np2}\right)},$$

$$\sigma_{\text{thnf}} = \frac{\left(\sigma_{np3}+2\sigma_{hnf}-2\phi_3\left(\sigma_{hnf}-\sigma_{np3}\right)\right)\sigma_{hnf}}{\sigma_{np3}+2\sigma_{hnf}+\phi_3\left(\sigma_{hnf}-\sigma_{np3}\right)}.$$

Table 1 — Thermophysical characteristics of *Cu, Fe_3O_4, Ti* and *Blood*[29]

Physical properties	$\rho\left(\frac{kg}{m^3}\right)$	$C_p\left(\frac{J}{kg\,K}\right)$	$k\left(\frac{W}{m\,K}\right)$	$\sigma\left(\Omega^{-1}m^{-1}\right)$	$\beta_T\times10^{-5}\left(\frac{1}{K}\right)$	Pr
Blood	1050	3167	0.52	0.8	1.8×10^{-1}	21
Cu	8933	385	400	5.96×10^{7}	17×10^{-1}	
Fe_3O_4	5200	670	6	25000	1.3	
Ti	4510	540	20	2.5×10^{6}	0.9	

Dynamic viscosity

$$\frac{\mu_{\text{thnf}}}{\mu_{\text{bf}}}=\frac{1}{\left(1-\phi_1\right)^{2.5}\left(1-\phi_2\right)^{2.5}\left(1-\phi_3\right)^{2.5}} \quad \ldots (6)$$

where ϕ_1, ϕ_2, and ϕ_3, are the volume fraction of *Cu* (Copper), Fe_3O_4(Iron oxide), and *Ti*(Titanium) nanoparticles, respectively. The suffix $thnf$, $np1, np2, np3$ and bf represents ternary hybrid nanofluid, solid nanoparticles of *Cu* (Copper), Fe_3O_4 (Iron oxide) and *Ti*(Titanium), nanoparticles, and the base fluid, respectively. Table 1 represents the principal amounts of thermophysical quantities for the nanoparticles and base fluids.

The PDEs listed in Eqs. (1)-(3) are modified into coupled, nonlinear ODEs by employing the pursuing similarity variables[2,5]:

$$\zeta=\left(\sqrt{\frac{(n+1)U_0}{2\gamma_f}}\right)\left\{\sqrt{(x+c)}\right\}^{(-1+n)}y,\psi=\sqrt{\frac{2\gamma_f U_0}{n+1}}\left\{\sqrt{(c+x)}\right\}^{(1+n)}$$
$$F(\zeta),\Theta(\zeta)=\frac{T-T_\infty}{T_w-T_\infty},u=U_0(x+c)^nF'(\zeta),$$
$$v=-\sqrt{\frac{\gamma_f(n+1)U_0}{2}}\left\{\sqrt{(x+c)}\right\}^{(n-1)}$$
$$\left(\zeta\frac{n-1}{n+1}F'(\zeta)+F(\zeta)\right), \quad \ldots (7)$$

The following is the reconstruction of Eqns. (2)-(4) using Eqns. (5)-(7).

$$\left.\begin{aligned}&\frac{\mu_{thnf}}{\mu_{bf}}\left(1+\frac{1}{\beta}\right)\left(\frac{n+1}{2}\right)F'''-\frac{\rho_{thnf}}{\rho_{bf}}\left[nF'^2-\left(\frac{n+1}{2}\right)F''F+F_sF'^2\right]+\\&\frac{(\rho\beta_T)_{thnf}}{(\rho\beta_T)_{bf}}\cos(\alpha)Gr\Theta\\&-\frac{\sigma_{thnf}}{\sigma_{bf}}M\left[F'-E\right]-K\frac{\mu_{thnf}}{\mu_{bf}}\left(1+\frac{1}{\beta}\right)F'=0,\end{aligned}\right\} \quad \ldots (8)$$

$$\left.\begin{aligned}&\frac{1}{\Pr}\left(\frac{k_{thnf}}{k_{bf}}+\frac{4}{3}R\right)\left(\frac{n+1}{2}\right)\Theta''+\frac{(\rho C_p)_{thnf}}{(\rho C_p)_{bf}}\left(\left(\frac{n+1}{2}\right)F\Theta'+\frac{n-1}{2}F'\Theta\right)\\&-\Gamma_t\frac{(\rho C_p)_{thnf}}{(\rho C_p)_{bf}}\left(\begin{aligned}&\frac{(n-1)^2}{2}\zeta^2FF''\Theta'+\left(\frac{n-1}{2}\right)\left(\frac{n+1}{2}\right)FF''\Theta+\left(\frac{n+1}{2}\right)^2F^2\Theta''\\&+(n-1)\left(\frac{3n-1}{2}\right)\zeta F'^2\Theta'-\left(\frac{n-1}{2}\right)^2F'^2\Theta+\left(\frac{n+1}{2}\right)\left(\frac{3n-1}{2}\right)FF'\Theta'\end{aligned}\right)\\&+\frac{\mu_{thnf}}{\mu_{bf}}\left(1+\frac{1}{\beta}\right)\left(\frac{n+1}{2}\right)EcF''^2+\frac{\sigma_{thnf}}{\sigma_{bf}}MEc\left[F'-E\right]^2+Q\Theta=0.\end{aligned}\right\} \quad \ldots (9)$$

The required boundary conditions are as follows[12]:

$$F'(\zeta)=1,F(\zeta)=\lambda\left(\frac{1-n}{1+n}\right),$$
$$-\sqrt{\frac{n+1}{2}}\frac{k_{thnf}}{k_f}\Theta'(\zeta)=Bi\left(1-\Theta(\zeta)\right), \quad \ldots (10)$$
$$\text{at } \zeta=\lambda,F'\to0,$$
$$\Theta\to0,\text{as}\,\zeta\to\infty.$$

Nonlinear and coupled, Eqs (8)-(10) have the domain $[\lambda,\infty]$. It should be converted to $[0,\infty]$ to facilitate the computations. Thus, we get[29]

$$F(\zeta)=f(\zeta-\lambda)=f(\eta),\theta(\zeta)=\theta(\zeta-\lambda)=\theta(\eta), \quad \ldots (11)$$

Here, Eqs. (8)-(10) as,

$$\left.\begin{aligned}&\frac{\mu_{thnf}}{\mu_{bf}}\left(1+\frac{1}{\beta}\right)\left(\frac{n+1}{2}\right)f'''-\frac{\rho_{thnf}}{\rho_{bf}}\left[nf'^2-\left(\frac{n+1}{2}\right)f''f+F_sf'^2\right]\\&+\frac{(\rho\beta_T)_{thnf}}{(\rho\beta_T)_{bf}}\cos(\alpha)Gr\theta-\frac{\sigma_{thnf}}{\sigma_{bf}}M\left[f'-E\right]-\\&K\frac{\mu_{thnf}}{\mu_{bf}}\left(1+\frac{1}{\beta}\right)f'=0,\end{aligned}\right\} \quad \ldots (12)$$

$$\left.\begin{aligned}&\frac{1}{\Pr}\left(\frac{k_{thnf}}{k_{bf}}+\frac{4}{3}R\right)\left(\frac{n+1}{2}\right)\theta^{*}+\frac{(\rho C_p)_{thnf}}{(\rho C_p)_{bf}}\left(\left(\frac{n+1}{2}\right)f\theta^{'}+\frac{n-1}{2}f^{'}\theta\right)\\&-\Gamma_t\frac{(\rho C_p)_{thnf}}{(\rho C_p)_{bf}}\left(\begin{aligned}&\frac{(n-1)^2}{2}\zeta^2 f f^{''}\theta^{'}+\left(\frac{n-1}{2}\right)\left(\frac{n+1}{2}\right)f f^{''}\theta+\left(\frac{n+1}{2}\right)^2 f^2\theta^{''}\\&+(n-1)\left(\frac{3n-1}{2}\right)\zeta f^{'2}\theta^{'}-\left(\frac{n-1}{2}\right)^2 f^{'2}\theta+\left(\frac{n+1}{2}\right)\left(\frac{3n-1}{2}\right)f f^{'}\theta^{'}\end{aligned}\right)\\&+\frac{\mu_{thnf}}{\mu_{bf}}\left(1+\frac{1}{\beta}\right)\left(\frac{n+1}{2}\right)Ecf^{''2}+\frac{\sigma_{thnf}}{\sigma_{bf}}MEc\left[f^{'}-E\right]^2+Q\theta=0.\end{aligned}\right\} \quad \ldots (13)$$

These are the necessary boundary conditions[12,29]:

$$\left.\begin{aligned}&f^{'}(\zeta)=1, f(\zeta)=\lambda\left(\frac{1-n}{1+n}\right),\\&-\sqrt{\frac{n+1}{2}}\frac{k_{thnf}}{k_f}\theta^{'}(\zeta)=Bi\left(1-\theta(\zeta)\right),\\&\text{at } \zeta=\lambda,\\&f^{'}\to 0,\theta\to 0,\text{as}\,\zeta\to\infty.\end{aligned}\right\} \quad \ldots (14)$$

Where α is the angle of inclined surface, $\Gamma_t=U_0(x+c)\varepsilon_t$ is the thermal relaxation time, $\lambda=\sqrt{\frac{n+1}{2}}\sqrt{\frac{U_0}{\upsilon_f}}J$ is the wall thickness variable, $Bi=\frac{h_f}{k_f}\sqrt{\frac{\upsilon_f}{U_0}}(x+c)^{\frac{1-n}{2}}$ is the Biot numbers, $M=\frac{\sigma B_0^2}{\rho_f U_0}$, is the magnetic field parameter, $E=\frac{E_0}{B_0u_w(x+c)^{\frac{n-1}{2}}}$, is the electric field, $K=\frac{\nu_f}{k_0^{'}U_0}$ is the porosity parameter, $F_s=\frac{u_wF^*}{U_0k_0^{'}}$ is the inertia coefficient, $Pr=\frac{\mu_f c_p}{k_f}$ is the Prandtl number, $R=\frac{4\sigma^*T_\infty^3}{k_fk^*}$ is the thermal radiation, $Gr=\frac{g(\beta_T)_{bf}(x+c)(T_w-T_\infty)}{u_w^2}$ is the Grashof number, $Ec=\frac{u_w^2}{(c_p)_{bf}(T_w-T_\infty)}$ is the Eckert number, $Q=\frac{Q_0}{(\rho c_p)_{bf}U_0}$ is the heat generation parameter.

The rate of transmission of heat and the skin friction coefficient are analysed to satisfy engineering curiosity:

$$\left.\begin{aligned}&C_f\,\mathrm{Re}_x^{1/2}\big/2=\sqrt{\left(\frac{1+n}{2}\right)}\frac{\mu_{thnf}}{\mu_{bf}}\left(1+\frac{1}{\beta}\right)f^{''}(0),\\&Nu_x\,\mathrm{Re}_x^{-1/2}=-\sqrt{\left(\frac{1+n}{2}\right)}\left(\frac{k_{thnf}}{k_{bf}}+\frac{4}{3}R\right)\theta^{'}(0).\end{aligned}\right\} \quad \ldots (15)$$

Here $\mathrm{Re}_x=\frac{(x+c)u_w}{\upsilon_f}$ represents the local Reynolds number.

Graphical Description

Using a graphical representation, we examined the non-dimensional parameters for the velocity and temperature profile $f'(\eta)$ and $\theta(\eta)$) data in this section. The consequences of the porosity parameter K on the $f'(\eta)$ and $\theta(\eta)$ when $n=0.5\,and\,1.5$ are described in Fig 2. In Fig. 2(a), the velocity decreases as the porosity parameter (K) values increase at $n=0.5\,and\,1.5$. It is also observed that the velocity is lower at $n=0.5$ compared to $n=1.5$. Fig. 2(b) illustrates that the higher porosity improves the temperature. This implies that the larger values of the porosity parameter lead to a thicker TBL.

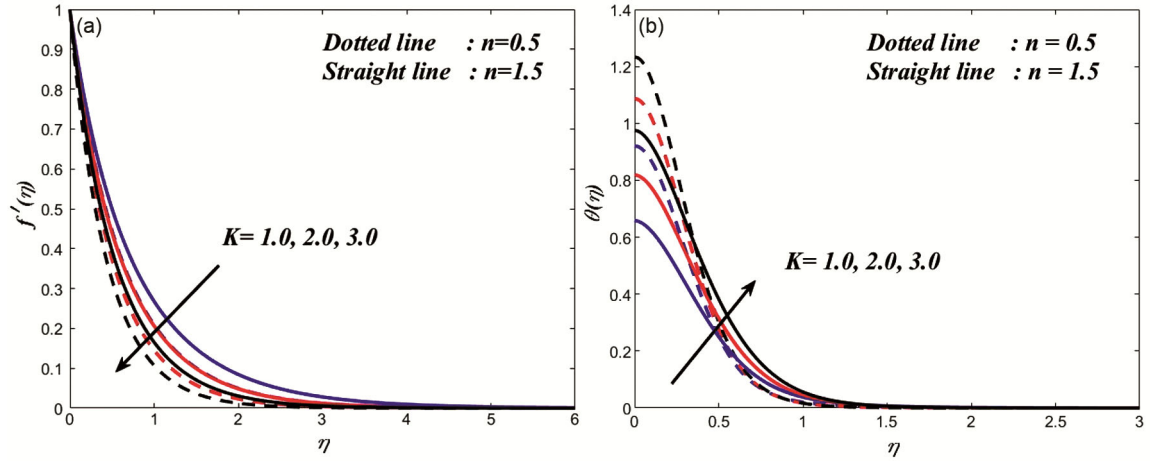

Fig. 2 — Graph for effect of K on (a) $f'(\eta)$ and (b) $\theta(\eta)$

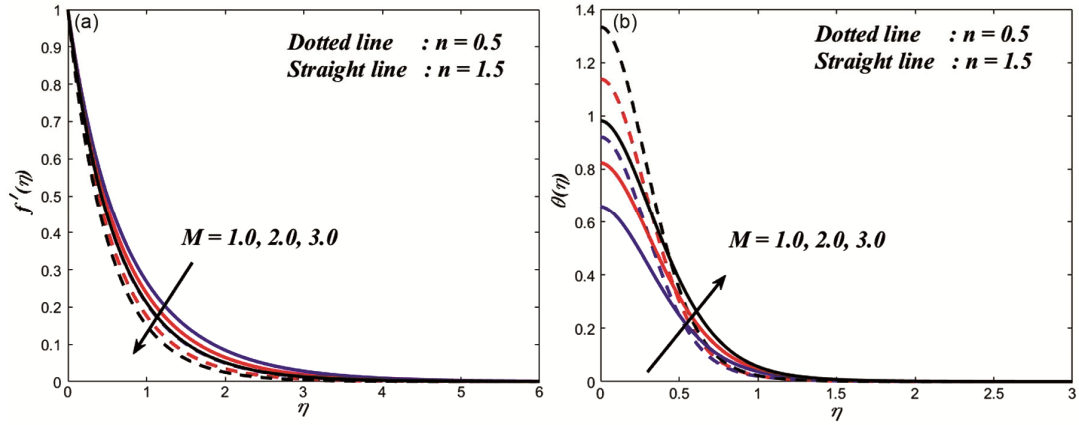

Fig. 3 — Graphs for effect of M on (a) $f'(\eta)$ and (b) $\theta(\eta)$

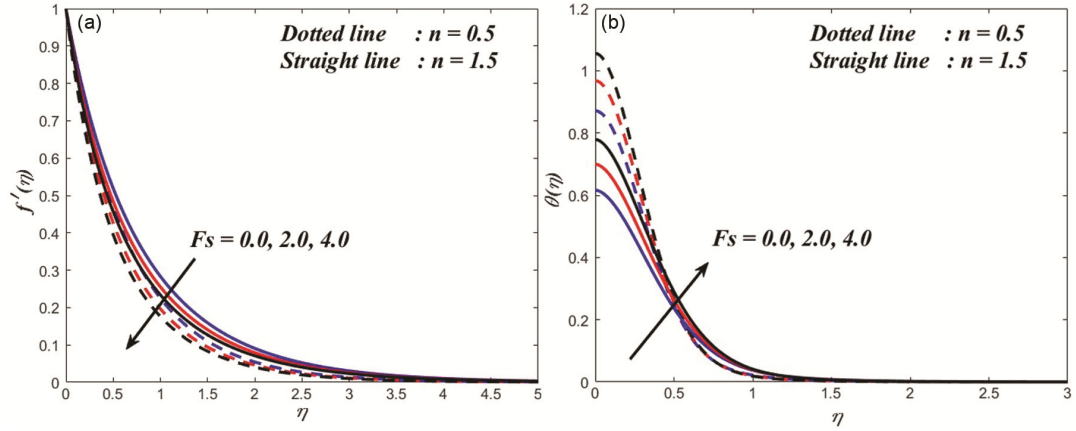

Fig. 4 — Graphs for effect of inertial coefficient F_s on (a) $f'(\eta)$ and (b) $\theta(\eta)$

The effect on THNF $f'(\eta)$ and $\theta(\eta)$ of the magnetic field (M) parameter is shown in Fig. 3. The velocity profile and the TBL decrease when the magnetic field (M) increases at $n = 0.5$ and $n = 1.5$ in Fig. 3(a). From Fig. 3(b), we find that the temperature for larger values of the magnetic field (M) rises on $n = 0.5$ and $n = 1.5$ which in turn raises the TBL thickness. This is due to the Lorentz force, which has already been studied in the existing literature[29].

The discrepancies of the inertial coefficient F_s on $f'(\eta)$ and $\theta(\eta)$ at $n = 0.5 \, and \, 1.5$ graphs are displayed in Fig. 4 for the ternary hybrid nanofluids. In Fig. 4, increasing the inertial coefficient lowers the velocity profiles, and the temperature shows a contradiction in THNF. Fig. 5 depicts the CF parameter (β) on $f'(\eta)$ and $\theta(\eta)$ at $n = 0.5 \, and \, 1.5$. Fig. 5(a) shows that fluid velocity decreases with an increase in the Casson fluid parameter, while Fig. 5(b) indicates that the temperature profile also decreases as the Casson fluid parameter increases.

The consequences of the Eckert number (Ec) on $f'(\eta)$ and $\theta(\eta)$ at $n = 0.5 \, and \, 1.5$ are displayed in Fig. 6. In Fig. 6(a), the velocity profile increases with a rise in Eckert number. The thermal profile rises with a rise in the Eckert number displayed in Fig. 6 (b). In Fig. 7(a) represents the influence of the Biot number (Bi) on $\theta(\eta)$ at $n = 0.5 \, and \, 1.5$. When the Biot number is higher, it increases the temperature profile. Fig. 7(b) shows that the effect of the heat generation parameter (Q) for the $\theta(\eta)$ when $n = 0.5 \, and \, 1.5$. The temperature profile increases when increasing the heat generation parameter for THNF.

Table 2 explains the rate of HT $Nu_x \, \mathrm{Re}_x^{-1/2}$ and skin friction coefficient $C_f \, \mathrm{Re}_x^{1/2} / 2$ for the different values of the parameters $n, \beta, \alpha, F_s, G_r, M, K, E,$

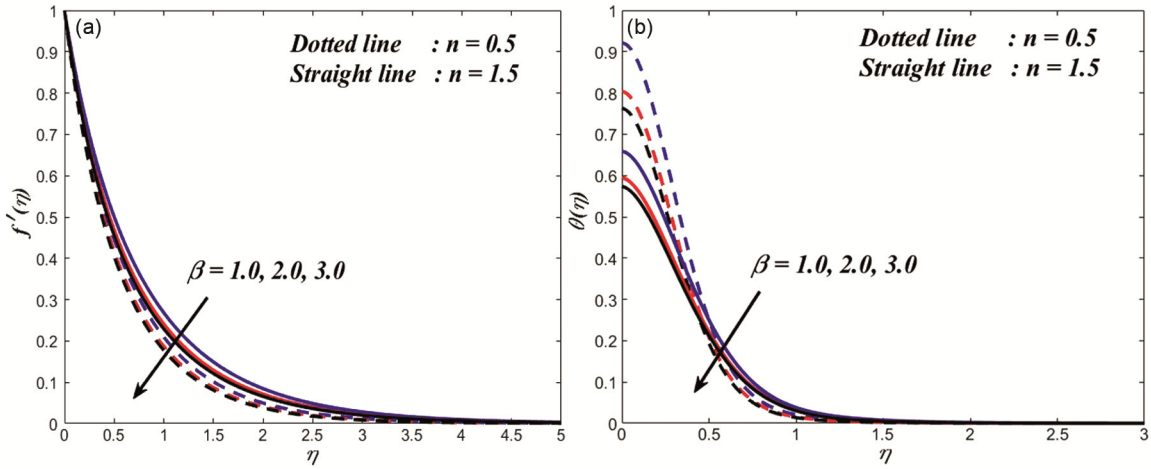

Fig. 5 — Graphs for effects of β on (a) $f'(\eta)$ and (b) $\theta(\eta)$

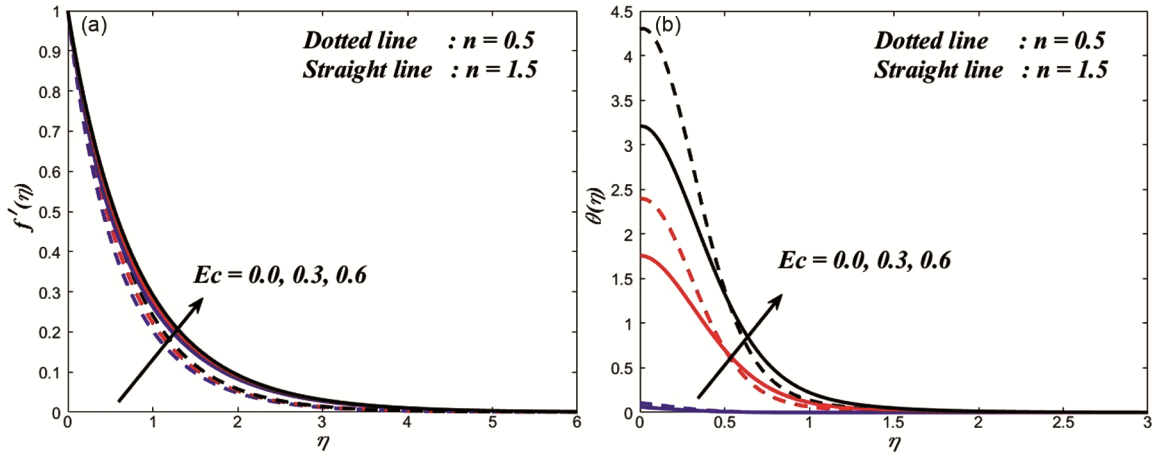

Fig. 6 — Graphs for effects of Ec on (a) $f'(\eta)$ and (b) $\theta(\eta)$

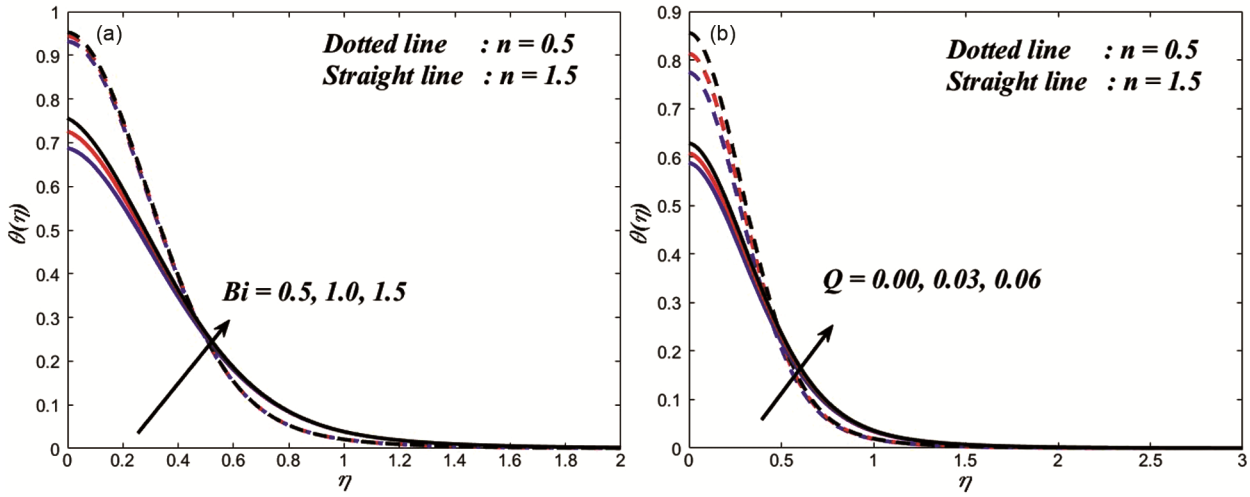

Fig. 7 — Graphs for (a) influence of the Biot number (Bi) on $\theta(\eta)$ and (b) heat generation parameter (Q) on $\theta(\eta)$ at $n = 0.5$ *and* 1.5

Table 2 — Numerical values of $f''(0)$ and $-\theta'(0)$ for various values of the $n,\beta,\alpha,F_s,G_r,M,K,\ E,\lambda,B_i,\Gamma_t,R,Ec$ and Q

n	β	α	F_s	G_r	M	K	E	λ	B_i	Γ_t	R	Ec	Q	$f''(0)$	$-\theta'(0)$
0.5	1.0	$\frac{\pi}{3}$	1.0	0.5	1.0	1.0	0.01	0.5	0.2	0.1	0.5	0.1	0.1	-1.6000	0.0269
1.5	1.0	$\frac{\pi}{3}$	1.0	0.5	1.0	1.0	0.01	0.5	0.2	0.1	0.5	0.1	0.1	-1.8053	0.1112
2.5	1.0	$\frac{\pi}{3}$	1.0	0.5	1.0	1.0	0.01	0.5	0.2	0.1	0.5	0.1	0.1	-1.9695	0.1221
0.5	1.5	$\frac{\pi}{3}$	1.0	0.5	1.0	1.0	0.01	0.5	0.2	0.1	0.5	0.1	0.1	-1.7006	0.0519
0.5	2.0	$\frac{\pi}{3}$	1.0	0.5	1.0	1.0	0.01	0.5	0.2	0.1	0.5	0.1	0.1	-1.7660	0.0648
0.5	2.5	$\frac{\pi}{3}$	1.0	0.5	1.0	1.0	0.01	0.5	0.2	0.1	0.5	0.1	0.1	-1.8120	0.0726
0.5	1.0	0	1.0	0.5	1.0	1.0	0.01	0.5	0.2	0.1	0.5	0.1	0.1	-1.5209	0.0363
0.5	1.0	$\frac{\pi}{4}$	1.0	0.5	1.0	1.0	0.01	0.5	0.2	0.1	0.5	0.1	0.1	-1.5668	0.0309
0.5	1.0	$\frac{\pi}{2}$	1.0	0.5	1.0	1.0	0.01	0.5	0.2	0.1	0.5	0.1	0.1	-1.6835	0.0166
0.5	1.0	$\frac{\pi}{3}$	1.5	0.5	1.0	1.0	0.01	0.5	0.2	0.1	0.5	0.1	0.1	-1.6648	0.0192
0.5	1.0	$\frac{\pi}{3}$	2.0	0.5	1.0	1.0	0.01	0.5	0.2	0.1	0.5	0.1	0.1	-1.7271	0.0116
0.5	1.0	$\frac{\pi}{3}$	2.5	0.5	1.0	1.0	0.01	0.5	0.2	0.1	0.5	0.1	0.1	-1.7872	0.0043
0.5	1.0	$\frac{\pi}{3}$	1.0	0.2	1.0	1.0	0.01	0.5	0.2	0.1	0.5	0.1	0.1	-1.6495	0.0208
0.5	1.0	$\frac{\pi}{3}$	1.0	0.3	1.0	1.0	0.01	0.5	0.2	0.1	0.5	0.1	0.1	-1.6329	0.0229
0.5	1.0	$\frac{\pi}{3}$	1.0	0.4	1.0	1.0	0.01	0.5	0.2	0.1	0.5	0.1	0.1	-1.6164	0.0249
0.5	1.0	$\frac{\pi}{3}$	1.0	0.5	0.2	1.0	0.01	0.5	0.2	0.1	0.5	0.1	0.1	-1.4686	0.0884
0.5	1.0	$\frac{\pi}{3}$	1.0	0.5	0.4	1.0	0.01	0.5	0.2	0.1	0.5	0.1	0.1	-1.5026	0.0723
0.5	1.0	$\frac{\pi}{3}$	1.0	0.5	0.6	1.0	0.01	0.5	0.2	0.1	0.5	0.1	0.1	-1.5358	0.0568
0.5	1.0	$\frac{\pi}{3}$	1.0	0.5	1.0	0.6	0.01	0.5	0.2	0.1	0.5	0.1	0.1	-1.4407	0.0448
0.5	1.0	$\frac{\pi}{3}$	1.0	0.5	1.0	0.7	0.01	0.5	0.2	0.1	0.5	0.1	0.1	-1.4823	0.0328

(*Contd.*)

Table 2 — Numerical values of $f''(0)$ and $-\theta'(0)$ for various values of the $n, \beta, \alpha, F_s, G_r, M, K, E, \lambda, B_i, \Gamma_t, R, Ec$ and Q (*Contd.*)

n	β	α	F_s	G_r	M	K	E	λ	B_i	Γ_t	R	Ec	Q	$f''(0)$	$-\theta'(0)$
0.5	1.0	$\frac{\pi}{3}$	1.0	0.5	1.0	08	0.01	0.5	0.2	0.1	0.5	0.1	0.1	-1.5227	0.0387
0.5	1.0	$\frac{\pi}{3}$	1.0	0.5	1.0	1.0	0.02	0.5	0.2	0.1	0.5	0.1	0.1	-1.5969	0.0290
0.5	1.0	$\frac{\pi}{3}$	1.0	0.5	1.0	1.0	0.03	0.5	0.2	0.1	0.5	0.1	0.1	-1.5937	0.0310
0.5	1.0	$\frac{\pi}{3}$	1.0	0.5	1.0	1.0	0.04	0.5	0.2	0.1	0.5	0.1	0.1	-1.5903	0.0328
0.5	1.0	$\frac{\pi}{3}$	1.0	0.5	1.0	1.0	0.01	0.6	0.2	0.1	0.5	0.1	0.1	-1.6103	0.0556
0.5	1.0	$\frac{\pi}{3}$	1.0	0.5	1.0	1.0	0.01	0.7	0.2	0.1	0.5	0.1	0.1	-1.6189	0.0800
0.5	1.0	$\frac{\pi}{3}$	1.0	0.5	1.0	1.0	0.01	0.8	0.2	0.1	0.5	0.1	0.1	-1.6262	0.1012
0.5	1.0	$\frac{\pi}{3}$	1.0	0.5	1.0	1.0	0.01	0.5	0.3	0.1	0.5	0.1	0.1	-1.5997	0.0384
0.5	1.0	$\frac{\pi}{3}$	1.0	0.5	1.0	1.0	0.01	0.5	0.4	0.1	0.5	0.1	0.1	-1.5995	0.0487
0.5	1.0	$\frac{\pi}{3}$	1.0	0.5	1.0	1.0	0.01	0.5	0.5	0.1	0.5	0.1	0.1	-1.5993	0.0582
0.5	1.0	$\frac{\pi}{3}$	1.0	0.5	1.0	1.0	0.01	0.5	0.2	0.04	0.5	0.1	0.1	-1.5931	0.0142
0.5	1.0	$\frac{\pi}{3}$	1.0	0.5	1.0	1.0	0.01	0.5	0.2	0.06	0.5	0.1	0.1	-1.5955	0.0185
0.5	1.0	$\frac{\pi}{3}$	1.0	0.5	1.0	1.0	0.01	0.5	0.2	0.08	0.5	0.1	0.1	-1.5978	0.0227
0.5	1.0	$\frac{\pi}{3}$	1.0	0.5	1.0	1.0	0.01	0.5	0.2	0.1	1.0	0.1	0.1	-1.6016	0.0803
0.5	1.0	$\frac{\pi}{3}$	1.0	0.5	1.0	1.0	0.01	0.5	0.2	0.1	1.5	0.1	0.1	-1.6021	0.1354
0.5	1.0	$\frac{\pi}{3}$	1.0	0.5	1.0	1.0	0.01	0.5	0.2	0.1	2.0	0.1	0.1	-1.6020	0.1912
0.5	1.0	$\frac{\pi}{3}$	1.0	0.5	1.0	1.0	0.01	0.5	0.2	0.1	0.5	0.07	0.1	-1.6225	0.1035
0.5	1.0	$\frac{\pi}{3}$	1.0	0.5	1.0	1.0	0.01	0.5	0.2	0.1	0.5	0.08	0.1	-1.6149	0.0778
0.5	1.0	$\frac{\pi}{3}$	1.0	0.5	1.0	1.0	0.01	0.5	0.2	0.1	0.5	0.09	0.1	-1.6075	0.0523

(*Contd.*)

Table 2 — Numerical values of $f''(0)$ and $-\theta'(0)$ for various values of the $n, \beta, \alpha, F_s, G_r, M, K, E, \lambda, B_i, \Gamma_t, R, Ec$ and Q (*Contd.*)

n	β	α	F_s	G_r	M	K	E	λ	B_i	Γ_t	R	Ec	Q	$f''(0)$	$-\theta'(0)$
0.5	1.0	$\frac{\pi}{3}$	1.0	0.5	1.0	1.0	0.01	0.5	0.2	0.1	0.5	0.1	0.07	-1.6048	0.0430
0.5	1.0	$\frac{\pi}{3}$	1.0	0.5	1.0	1.0	0.01	0.5	0.2	0.1	0.5	0.1	0.08	-1.6033	0.0378
0.5	1.0	$\frac{\pi}{3}$	1.0	0.5	1.0	1.0	0.01	0.5	0.2	0.1	0.5	0.1	0.09	-1.6017	0.0325

λ , Bi ,, Γ_t , R , Ec and Q. The $C_f \operatorname{Re}_x^{1/2} / 2$ decreases with increasing the inclination angle parameter, porosity parameter, and thermal relaxation time parameter, whereas opposite behaviour exists in the Biot number and Eckert number. The $Nu_x \operatorname{Re}_x^{-1/2}$ increases with increasing the Biot number, nanoparticle volume fraction and thermal relaxation time parameter, whereas opposite behaviour exists in inclination angle parameter, magnetic field parameter, Eckertnumber, and porosity parameter.Some additional significant trends are clearly illustrated in the contour plots presented in Figs. S1-S4 in Supplementary Information.

Conclusion

In the present study, two-dimensional nonlinear flow of ternary hybrid Casson nanofluid (Cu–Fe_3O_4–Ti/Blood) over an inclined stretching sheet with EMHD is considered, which gives immense performance in thermal conductivity. The given governing PDEs are transformed using similarity variables into coupled ODEs. The MATLAB bvp4c approach is used to examine the provided results. The main findings, along with their biomedical engineering relevance, are summarized as follows:

- An increase in the porosity parameter reduces the velocity but elevates the temperature profile, which is beneficial in controlled perfusion and porous biomedical scaffolds where enhanced thermal regulation is desired.
- Higher magnetic field strength increases temperature while reducing velocity, indicating potential for magnetic-field-assisted blood flow control in targeted hyperthermia and magnetic drug delivery systems.
- Increasing the Biot number raises the fluid temperature, and a similar trend is observed with the heat generation parameter; this behaviour is relevant to bioheat transfer processes such as tissue heating and thermal therapy.
- The Eckert number enhances both temperature and velocity profiles, reflecting the significance of viscous dissipation in high-shear biomedical flows such as blood pumping and microcirculatory transport.
- An increase in thermal relaxation time improves the heat transfer rate, which is important in accurately modelling non-Fourier heat conduction in biological tissues.
- The skin friction coefficient and heat transfer rate decrease with increasing inclination angle. Here, $\alpha = 0$ corresponds to a horizontal surface, $\alpha = \pi / 4$ to an inclined surface, and $\alpha = \pi / 2$ to a vertical surface. This observation is useful for the orientation-based design of biomedical flow and thermal management devices.

Overall, the present model may provide useful guidance for thedesign and optimization of advanced biomedical thermal systems, including targeted drug delivery, blood flow regulation, magnetic hyperthermia, and bioheat transfer devices.

Conflict of Interest

The authors declare that they have no conflict of interest.

Supplementary Information

Supplementary information is available on the website https://nopr.niscpr.res.in/handle/123456789.

References

Li W Khan S A Shafqat M Abbas Q Muhammad T & Imran M Computational analysis for efficient thermal transportation of ternary hybrid nanofluid flow across a stretching sheet with Cattaneo-Christov heat flux model, *Case Stud Therm Eng*, 66 (2025) 105706.

Reddy S R R & Anki R P B, Thermal radiation effect on unsteady three-dimensional MHD flow of micropolar fluid over a horizontal surface of a parabola of revolution, *Propul Power Res*, 11 (2022) 129

Sharjeel S & Sagheer M, Investigating MHD ternary nanofluid flow on a stretching sheet with cattaneo-christov

heat flux under thompson-troian slip condition: A yamada-ota model approach, *J Nanofluids*, 14 (2025) 48

Rani K S, Reddy G V R & Oke A S, Significance of cattaneo-christov heat flux on chemically reacting nanofluids flow past a stretching sheet with joule heating effect, *CFD Lett*, 15 (2023) 31.

Reddy S R R, Reddy P A & Rashad A M, Activation energy impact on chemically reacting eyring–powell nanofluid flow over a stretching cylinder, *Arab Sci Eng*, 45 (2020) 5227.

Abdal S, Siddique I, Ahmadian A, Salahshour S & Salimi M, Enhanced heat transportation for bioconvective motion of Maxwell nanofluids over a stretching sheet with Cattaneo-Christov flux, *Mech Time-Depend Mater*, 27 (2023) 1257.

Iqbal Z, Khan M, Shoaib M, Ahammad N A & Sidi M O, Heat transport analysis in buoyancy-driven flow of Maxwell fluid induced by a vertically stretching sheet inspired by CattaneoChristov theory, *Waves Random Complex Media*, 35 (2022) 12550.

Shankaralingappa B M, Prasannakumara B C, Gireesha B J & Sarris I E, The impact of cattaneo–christov double diffusion on oldroyd-b fluid flow over a stretching sheet with thermophoretic particle deposition and relaxation chemical reaction, *Inventions*, 6 (2021) 95.

Abbas W, Megahed A M, Morsy O M, Ibrahim M A & Said A A M, Dissipative Williamson fluid flow with double diffusive Cattaneo-Christov model due to a slippery stretching sheet embedded in a porous medium, *AIMS Math*, 7 (2022) 20781.

Khalil K M, Soleiman A, Megahed A M & Abbas W, Impact of variable fluid properties and double diffusive cattaneo-christov model on dissipative non-newtonian fluid flow due to a stretching sheet, *Mathematics*, 10 (2022) 1179.

Abbas N, Shatanawi W & Shatnawi T A M, Numerical analysis of a chemically reactive non-Newtonian nanofluid flow over an exponentially stretching curved Riga sheet, *Partial Differ Equ Appl Math*, 14 (2025) 101170.

Elgazery N S & Elelamy A F, Multiple solutions for non-Newtonian nanofluid flow over a stretching sheet with nonlinear thermal radiation: Application in transdermal drug delivery, *Pramana J Phys*, 94 (2020) 68.

Reddy S R R & Reddy P B A, Numerical simulations of unsteady 3D MHD micropolar fluid flow over a slendering sheet, *J Appl Comput Mech*, 7 (2021) 1403.

Tarakaramu N, Satya N P V, Sivakumar N, Harish B D & Bhagya L K, Convective conditions on 3D magneto hydrodynamic (MHD) non-newtonian nanofluid flow with nonlinear thermal radiation and heat absorption: A numerical analysis, *J Nanofluids*, 12 (2022) 448.

Tuesday K, Kinyanjui M N & Giterere K, Unsteady hydromagnetic non-newtonian nanofluid flow past a porous stretching sheet in the presence of variable magnetic field and chemical reaction, *J Appl Math Phys*, 11 (2023) 2545.

Reddy S R R & Reddy P B A, Impact of thermal radiation and viscous dissipation on hydromagnetic unsteady flow over an exponentially inclined preamble stretching sheet, *J Comput Appl Res Mech Eng*, 10 (2020) 171.

Amer A M, Ghoneim N I & Megahed A M, Investigation of dissipation phenomenon of non-Newtonian nanofluid due to a horizontal stretching rough sheet through a Darcy porous medium, *Appl Eng Sci*, 17 (2024) 100171.

Xin X, Ganie A H, Alwuthaynani M, Bonyah E, El-Wahed K H A, Fathima D & Bilal M, Parametric analysis of pollutant discharge concentration in non-Newtonian nanofluid flow across a permeable Riga sheet with thermal radiation, *AIP Adv*, 14 (2024) 045018.

Ramesh K, Asogwa K K, Oreyeni T, Reddy M G & Verma A, EMHD radiative titanium oxide-iron oxide/ethylene glycol hybrid nanofluid flow over an exponentially stretching sheet, *Biomass Conv Bioref*, 14 (2024) 18887.

Abbas N, Rehman K U, Shatanawi W & Al-Eid A A, Theoretical study of non-Newtonian micropolar nanofluid flow over an exponentially stretching surface with free stream velocity, *Adv Mech Eng*, 14 (2022) 1.

Yousef N S, Megahed A M, Ghoneim N I, Elsafi M & Fares E, Chemical reaction impact on MHD dissipative Casson-Williamson nanofluid flow over a slippery stretching sheet through porous medium, *Alex Eng J*, 61 (2022) 10161.

Mondal H, Pal D, Chatterjee S & Sibanda P, Thermophoresis and soret-dufour on MHD mixed convection mass transfer over an inclined plate with non-uniform heat source/sink and chemical reaction, *Ain Shams Eng J*, 9 (2018) 2111.

Amer A M, Ghoneim N I & Megahed A M, Investigation of dissipation phenomenon of non-Newtonian nanofluid due to a horizontal stretching rough sheet through a Darcy porous medium, *Appl Eng Sci*, 17 (2024) 100171.

Raza J, Mebarek-Oudina F & Mahanthesh B, (Magneto hydrodynamic flow of nano Williamson fluid generated by stretching plate with multiple slips, *Multidiscip Model Mater Struct*, 15 (2019) 871.

Ekang I F, Joshua E E, Senge I O & Nyong E, MHD Casson fluid flow with chemical reaction and suction in a porous medium over an exponentially stretching sheet, *World J Appl Sci Technol*, 15 (2023) 43.

Kayalvizhi J & Kumar A V G, Entropy analysis of EMHD hybrid nanofluid stagnation point flow over a porous stretching sheet with melting heat transfer in the presence of thermal radiation, *Energies*, 15 (2022) 8317.

Qamar I, Farooq M A, Irfan M & Mushtaq A, Insight into the dynamics of electro-magneto-hydrodynamic fluid flow past a sheet using the Galerkin finite element method: Effects of variable magnetic and electric fields, *Frontiers in Physics*, 10 (2022) 1.

Salah F, Sidahmed A O M & Viswanathan K K, Chemical MHD hiemenz flow over a nonlinear stretching sheet and brownian motion effects of nanoparticles through a porous medium with radiation effect, *Math Comput Appl*, 28 (2023) 21.

Jakeer S, Reddy S R R, Rashad A M, Lakshmi R M & Manjula C, Nonlinear analysis of darcy-forchheimer flow in EMHD ternary hybrid nanofluid (Cu-CNT-Ti/water) with radiation effect, *Forces Mech*, 10 (2023) 100177.